Photon-counting with single stoichiometric TiN layer-based optical MKIDs

Faouzi Boussaha, Jie Hu, Paul Nicaise, Jean-Marc Martin, Christine Chaumont, Pham Viet Dung, Josiane Firminy, Florent Reix, Piercarlo Bonifacio, Michel Piat, et al.

▶ **To cite this version:**

Faouzi Boussaha, Jie Hu, Paul Nicaise, Jean-Marc Martin, Christine Chaumont, et al.. Photon-counting with single stoichiometric TiN layer-based optical MKIDs. Applied Physics Letters, 2023, 122 (21), 10.1063/5.0147584 . hal-04263305

HAL Id: hal-04263305
https://hal.science/hal-04263305v1

Submitted on 28 Oct 2023

HAL is a multi-disciplinary open access archive for the deposit and dissemination of scientific research documents, whether they are published or not. The documents may come from teaching and research institutions in France or abroad, or from public or private research centers.

L'archive ouverte pluridisciplinaire **HAL**, est destinée au dépôt et à la diffusion de documents scientifiques de niveau recherche, publiés ou non, émanant des établissements d'enseignement et de recherche français ou étrangers, des laboratoires publics ou privés.

Photon-counting with Single Stoichiometric TiN Layer-based Optical MKIDs

Faouzi Boussaha,[1] Jie Hu,[1,2] Paul Nicaise,[1] Jean-Marc Martin,[1] Christine Chaumont,[1] Pham Viet Dung,[2] Josiane Firminy,[1] Florent Reix,[1] Piercarlo Bonifacio,[1] Michel Piat,[2] and Hervé Geoffray[3]

[1)] *GEPI Observatoire de Paris - Université PSL, CNRS, 75014 Paris, France*

[2)] *Université de Paris Cité, CNRS, Astroparticule et Cosmologie, F-75013 Paris, France*

[3)] *French Space Agency CNES, 31400 Toulouse, France*

(*Electronic mail: faouzi.Boussaha@obspm.fr)

(Dated: 9 May 2023)

We demonstrate the single photon counting mode at 405 and 850 nm with stoichiometric TiN-based microwave kinetic inductance detectors realized on sapphire substrate and operated at bath temperatures over 300 mK. The detectors use single 15-25 nm-thick TiN layers featuring a critical temperature in the 2-3K range. We found that the energy-resolving power $R = E/\Delta E$ exhibits an optimum with bath temperature, occurring in the 300-450mK range, which can be almost double compared to those obtained at the lowest temperatures. Furthermore, the single photon regime is observed up to 700 mK. In addition to a high-temperature operation, the single stoichiometric layer would allow achieving a better uniformity in the critical temperature and thus kinetic inductance, compared to the often desired $\sim$ 1K sub-stoichiometric TiN.

Microwave kinetic inductance detector (MKID)[1] is currently one of the most promising superconducting sensor technologies, capable to address many applications in astronomy[2–5] and physics. It has already been demonstrated in astrophysics, where several instruments covering a large electromagnetic spectrum ranging from millimeter-submillimeter waves[3,6–8] to optical[2,9] and x-rays[10,11] have been implemented. An MKID is a superconducting *LC* resonator usually consisting of a meander as the inductor and an interdigital capacitor in the optical and near-infrared range. The detection is achieved when the absorbed photons ($h\nu > 2\Delta$, $\Delta = 1.76 k_B T_c$ is the energy gap of the superconductor of the inductor. k_B is the Boltzmann constant and T_c is the critical temperature) by the inductor L break the Cooper pairs into quasiparticles, modifying its resonance frequency and impedance. The performance of MKIDs depends to a large extent on the quality of the superconducting layer. The implementation and investigation of suitable superconductors to achieve ultimate performance is currently an important research area. In the optical and near-infrared wavelength range, superconducting materials with high normal resistivity and low critical temperature are favored, such as titanium nitride (TiN), platinum silicide (PtSi)[12], hafnium (Hf)[13] and beta phase tantalum (β-Ta)[14] to achieve better quantum efficiency as well as higher energy-resolving power as the sensitivity inversely proportional to the critical temperature T_c ($\propto /{T_c}^2$). TiN obtained by nitriding titanium can exhibit high resistivity (several hundred of $\mu\Omega \cdot$ cm) and large kinetic inductance L_k (a few dozen to a few hundred $pH/\square$) at a T_c that can be tuned between ~ 0.35 and 4.6 K. T_c depends on the amount of nitrogen reacting with Ti to form the TiN during the deposition[15], leading to two TiN states: sub-stoichiometric and stoichiometric. As reported elsewhere[15–17], one can consider that the stoichiometric state corresponds to the plateau above the steep slope that represents the measured critical temperature as a function of nitrogen flow, while the sub-stoichiometric state mainly concerns values directly in the steep slope, defined as the transition phase. The sub-stoichiometric TiN with T_c not lower than 0.8-1 K is preferred to improve the sensitivity as well as to meet cryogenics constraints. The first sub-stoichiometric TiN-based MKIDs demonstrating very promising performances, in terms of intrinsic resonance quality Q_i and sensitivity[18,19] have been reported. Nevertheless, it has two main drawbacks that can greatly hamper the realization of large arrays. On the one hand, the sub-stoichiometric TiN layer exhibits inhomogeneities in the critical temperature, and consequently, in the kinetic inductance L_k, leading ultimately to the occurrence of overlaps and collisions between resonances. Furthermore, unlike the stoichiometric layer, it usually shows larger losses when deposited on a sapphire substrate than on a silicon substrate due to lattice mismatch, while the latter should not be used especially in the 400-800 nm wavelength range to avoid photon absorption in the substrate, which could produce strong substrate event[18]. On the other hand, the transition from stoichiometric to sub-stoichiometric TiN with respect to nitrogen flow is very sharp, which makes the T_c not so controllable. In this case, TiN/Ti/TiN[16,20,21], PtSi[12], and Hf are investigated to improve the homogeneity to the superconducting films as well as the energy-resolving power. However, PtSi needs a specific fabrication process whereas Hf, which features a very low critical temperature of $\sim$ 0.4 K, requires the use of a more powerful cryostat to go down to about 15-20 mK[13]. This can present a significant challenge for building large-scale arrays. So far, most reported MKIDs are deposited with $T_c \sim 1$ K and are operated at a low bath temperature around $T \approx 100$ mK and below, as it is well known that at least $T < T_c/8$ is required to achieve the high detection performance. In this case, a dilution cryostat or an adiabatic demagnetization refrigerator (ADR) is needed.

In this letter, we investigate the possibility of using a single-layer stoichiometric TiN on sapphire to build sensitive MKID arrays operating in a single photon counting regime at temperatures well above 300 mK. Unlike sub-stoichiometric TiN, the T_c of stoichiometric layers varies very little with the fabrication parameters which likely contributes to achieving a better uniformity in the kinetic inductance. We designed an array

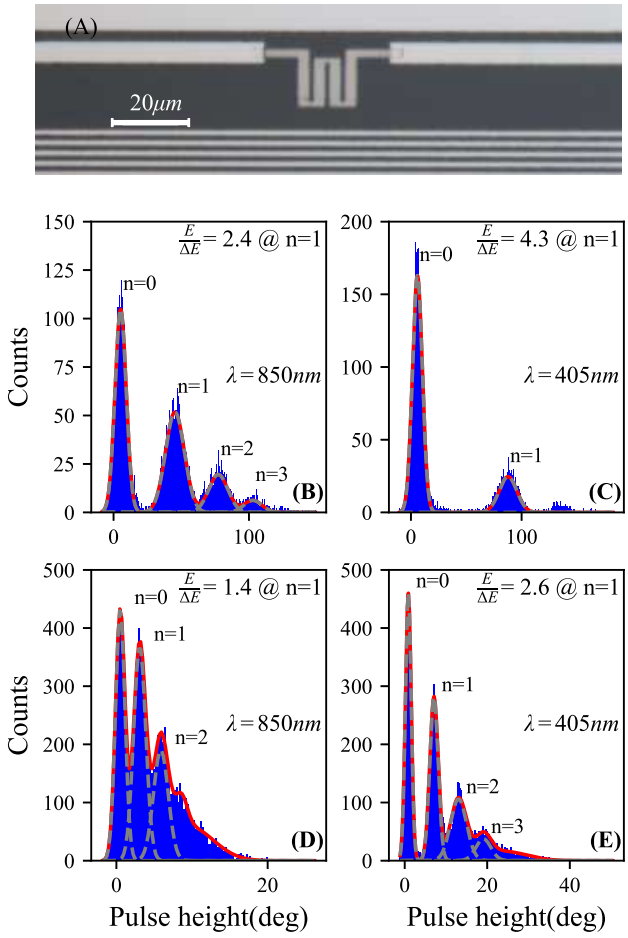

FIG. 1. (A) Optical picture showing one of the fabricated 6x6 MKIDs, which uses a meander of 2.8 μm^3. The volume of the meander is small to improve the sensitivity. (B-C) Histograms of phase response heights measured at 300 mK when the $TiN_{2.1K}$ MKID with 15 nm-thick, V=1.3 μm^3 and f_r=3.137 GHz is illuminated with short pulses at 405 and 850 nm wavelength, respectively. (D-E) Histograms of phase response heights of the $TiN_{3.8K}$ MKID with 25 nm-thick, V=2.8 μm^3 and f_r=4.078 GHz at 400 mK when it also illuminated at 405 and 850 nm, respectively. At these temperatures, their quality factors Q_i are $\sim 2.5\times10^4$ and 7.7×10^4, respectively. The dashed red-gray lines indicate the Gaussian fits.

of 6×6 MKIDs where each MKID is made up of a TiN meander in parallel with an Nb interdigitated capacitor (IDC) as illustrated in FIG. 1-(A). The two elements are connected with arms on either side of the meander that are shaped to improve the RF coupling between the resonator and the 50 Ω CPW line made from a 100 nm-thick Nb layer that reads out the resonators. The capacitors of 288×282 μm are also made of a 100 nm-thick Nb layer with a finger gap and width of 1.2 μm. Multiplexing is achieved by removing different portions of the IDC fingers so that each resonator has its unique resonance frequency. We fabricated two arrays that differ only by their thickness and critical temperature of the TiN inductive meander. The chosen T_c are, respectively, right after the steep

TABLE I. Main Parameters for TiN MKIDs

	T_c(k)	t (nm)	L_k (pH/□)	ρ_n ($\mu\Omega\cdot cm$)	Q_i
TiN_{2K}	2.1	15	61	140	2.5×10^4
TiN_{3K}	3.8	25	30	210	7.7×10^4

transition and on the plateau[17]. The first array uses a 15 nm-thick TiN layer to achieve a high kinetic inductance within the absorber. However, this thin film yields a lower T_c of around 2.1 K, instead of 3.8 K for a 60 nm-thick layer. Its resistivity is measured to be $\rho_{TiN_{2.1K}}\approx140$ $\mu\Omega\cdot$cm (RRR $\approx$ 1.1), yielding a $L_k=\rho\hbar/\Delta\pi t\approx61$ $pH/\square$, where $\hbar$ is the reduced Planck constant and t is the thickness. We carried out this study with two different meander volumes of V=1.3 and 2.8 μm^3 with areas of A=13.8×6.4 μm^2 and 13.8×13.5 μm^2, respectively. These meanders consist of strips of 2.7 μm-width and total length of 20 and 72 μm, respectively. This leads to resonance frequencies ranging from 1.96 to 3.2 GHz. The second array is made of a thicker TiN layer of 25 nm. In addition to the thickness, we also increased its T_c by changing only the nitrogen flow (an increase of $\sim$ 20%) during the TiN deposition. This allows to achieve $T_c\approx3.8$ K ($\sim$ 4.5 K for 60 nm-thick). Its measured $\rho_{TiN_{3.8K}}\approx210$ $\mu\Omega\cdot$cm gives $L_k\approx30$ $pH/\square$. The meander volumes become 2.16 and 4.6 μm^3, respectively, and resonance frequencies range from 2.9 to 4 GHz. For both arrays, the low Nb kinetic inductance of ~0.2 $pH/\square$ will greatly contribute to preventing the undesired responses from capacitors and the coupling arms. For clarity, the main parameters are summarized in Table I.

The arrays are fabricated on c-plane sapphire substrates. They are cooled in an ADR and characterized using the standard homodyne detection[22] in the 50-700 mK temperature range. Using the same fabrication process, the typical internal quality factors Q_i are 2.5×10^4 and 7.7×10^4 for $TiN_{2.1K}$ and $TiN_{3.8K}$ MKIDs, respectively. The coupling quality factor Q_c are around 2.5×10^4 and 4×10^4, respectively. Note that MKIDs fabricated from sub-stoichiometric 60 nm-thick TiN ($T_c\approx$ 1-1.4 K) layer deposited on sapphire substrate gave consistently much shallower resonances of maximum 1-2 dB with lower Q_i not exceeding 5×10^3. The power on the CPW readout line is always judiciously applied to avoid resonance bifurcation due to the non-linear regime.

The illumination is performed with two laser sources at 405 and 850 nm wavelength, respectively, through an optical fiber positioned at 35 mm above the array[22,23]. The MKIDs are subjected to a train of short pulses of 50-150 ns width at a frequency of 250 Hz. FIGs. 1-B-C show the typical histograms obtained for 10^4 optical pulse events at 300 mK with the $TiN_{2.1K}$ MKID resonating at f_r = 3.136 GHz. To assess whether these stoichiometric TiN-based MKIDs are able to achieve photon-counting, we employ the widely used Weiner optimal filter[19,20] to generate photon-counting statistics. The maximum energy-resolving power $R=E/\Delta E$ are 5 and 2.4 at 405 and 850 nm, respectively (see FIGs. 2-3). The applied

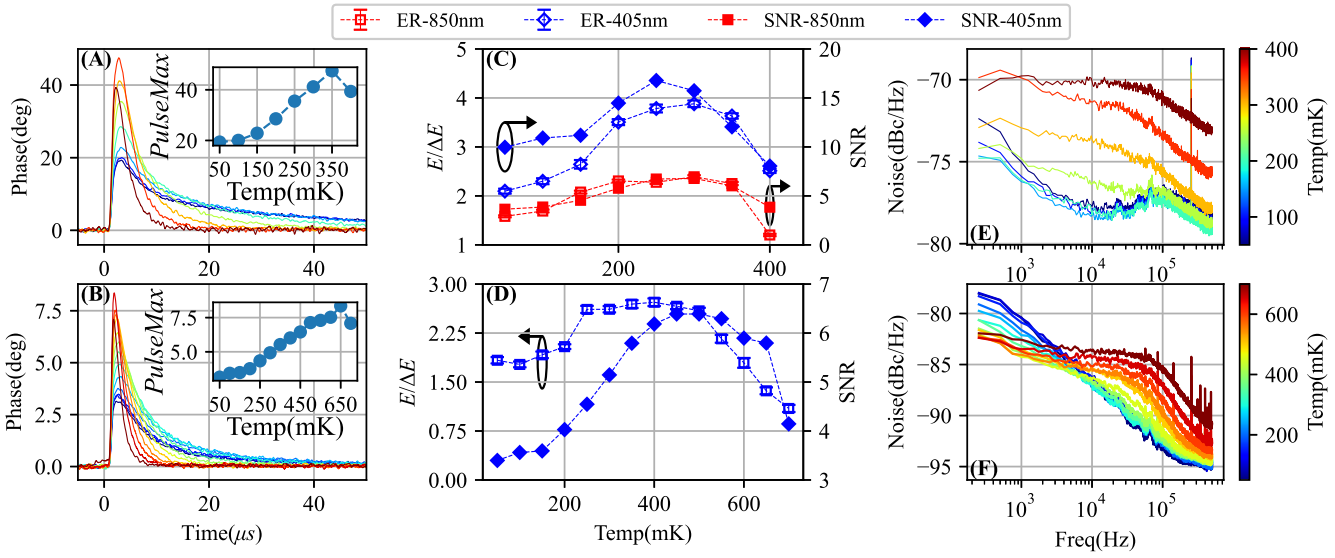

FIG. 2. Evolution of different measured parameters as a function of the temperature of a pixel of $TiN_{2.1K}$-15nm with V=2.8 μm^3 (A, C, E) and a pixel of $TiN_{3.8K}$-25nm with V=4.6 μm^3 (B, D, F): (A-B) Single photon pulses versus temperature. The insets show the pulse maximum versus temperature. (C): Energy-resolving power and signal-to-noise SNR versus temperature at 405 nm and 850 nm, respectively with $TiN_{2.1K}$-15nm. (D): Energy resolving power and signal-to-noise SNR versus temperature at 405 nm $TiN_{3.8K}$-25nm (measurements at 850 nm could not be carried out with the same MKID). (E-F): The phase noise versus temperature.

readout power on the CPW readout line is P_r=-98 dBm. Using both lasers, in FIGs. 1-D-E, we show histograms of the $TiN_{3.8K}$ MKID, with f_r=4.078 GHz, measured at 400 mK and P_r=-90 dBm. Due to the difference in T_c as well as in volume (both MKIDs obviously have the same geometry), the maximum $E/\Delta E$ is slightly smaller and is measured to be 3.8 at 405 nm (see FIG. 3). At 850 nm, we measured a maximum $E/\Delta E$ of 2.2 with the MKID of V=2.2 μm^3. Depending on the optical power absorbed in the MKIDs, we can notice that up to 4 peaks corresponding to n=0, 1, 2, and 3 photons can clearly be resolved. The full-width-at-half-maximum (FWHM) energy resolution ΔE=1.0 eV and 1.2 eV for n=1 and 2 at 850 nm, respectively. Furthermore, similar histograms are obtained up to 500 mK. The energy-resolving power is admittedly still far below the theoretical Fano limit[24] of more than 100 at 400 nm but can be considered in the same order of magnitude as those usually obtained so far with sub-stoichiometric TiN and TiN/Ti/TiN multilayer[16,20]. Note that this is without the use of quantum-limited parametric amplifier[13], a phonon trapping layer under the meander[24] or a suspended meander on a thin membrane[25] to trap photons within the meander to further enhance the Cooper pairs breaking, leading to the improvement of the energy-resolving power. Thus, the combination of stoichiometric TiN-based MKIDs with one or several of these approaches will lead to a significant performance improvement. This is particularly important for large meanders where $E/\Delta E$ can decrease dramatically. For example, the use of a parametric amplifier could greatly enhance $E/\Delta E$ by almost a factor of two.

In FIGs. 2-A-B, we present the single pulse response in the time domain as a function of the temperature of the two MKIDs when illuminated at 405 nm. The corresponding maximum quasi-particle lifetime τ_{qp} are measured to be around 22 and 13μs for, respectively, $TiN_{2.1K}$ and $TiN_{3.8K}$ MKIDs at 50 mK which are similar to those reported elsewhere[15,26], but much smaller than that of substoichiometric TiN layers which are usually in 50-100 μs[18] range when cooled at $<T_c/10$. $TiN_{2.1K}$ MKID which presents a higher τ_{qp} decreases with temperature more rapidly than $TiN_{3.8K}$ MKID to reach their minimum around 1μs from 400 and 700 mK, respectively. These short τ_{qp} can still be easily processed with our straightforward readout electronics. As we noticed that phase response heights $\Delta\varphi$ can increase with temperature as shown in Fig. 2-A-B, we plot as insets in the same figure, their maximum as a function of bath temperature.

The maximum $\Delta\varphi$ increases as MKIDs operate in the transient mode. In this case, $\Delta\varphi$ is related to the photon energy E and the energy gap $\Delta(T)$ as follows:[19]

$$\Delta\varphi \propto \frac{\eta E}{\Delta(T)} \tag{1}$$

where η is the photon absorption efficiency. Thus, $\Delta\varphi$ increases as $\Delta(T)$ decreases when the bath temperature rises. It should be noted that for an MKID operating in the steady state in the millimeter wave range[27], $\Delta\phi$ is different from (1), which is

$$\Delta\varphi \propto \frac{\tau_{qp}\eta E}{\Delta(T)} \tag{2}$$

Thus, when the bath temperature rises, τ_{qp} decreases resulting in $\tau_{qp}/\Delta(T) < 1$[1] and a reduction of phase response.

In FIGs. 2-C-D, we also present the energy-resolving power $R = E/\Delta E$ along with the signal-to-noise ratio (SNR) which

can be estimated as

$$SNR \propto \frac{P_{max}}{\sqrt{\int P_n df}} \quad (3)$$

where P_{max} is the pulse maximum as shown in Fig. 2-A-B, and P_n is the phase noise shown in Fig. 2-E-F. According to all these plots, we can distinguish 3 stages as a function of bath temperature.

The first stage which occurs at $T \sim 0.05T_c$, up to $\sim$ 150 mK for the $TiN_{2.1K}$ MKID and $\sim$ 200 mK for the $TiN_{3.8K}$ MKID, $E/\Delta E$ and $\Delta\varphi$ are small and roughly constant. In this temperature range, TLS dominates in two ways. First, it introduces a $1/f^{0.5}$ frequency-dependent noise for T<$T_c/10$ (see Fig. 2-E-F). Second, it affects the frequency shift through the capacitor, generating an undesired phase response in the opposite direction, which reduces the meander-based phase response, as was experimentally observed by J. Hu et al.[22]. The second stage is triggered when the TLS noise level starts to decrease (i.e., $1/f^{0.5}$ slope is less pronounced) from $\sim$ 150 mK and $\sim$ 200 mK, respectively, for the two MKIDs, while phase responses P_{max}, and therefore SNR, increase with bath temperature. Here, $E/\Delta E$ exhibits optimum in 200-350 mK and 250-500 mK ranges for, respectively, $TiN_{2.1K}$ and $TiN_{3.8K}$ with an improvement factor of 1.5-2 to the $E/\Delta E$ at 50 mK. This is comparable with the improvement in energy-resolving power obtained by using the superconducting parametric amplifier[13]. The third stage occurs, around $T_c/8$, beyond 350 mK for the $TiN_{2.1K}$ MKID and 500 mK for the $TiN_{3.8K}$ MKID where $E/\Delta E$ and $\Delta\varphi$ dramatically decrease due to the degradation of the signal-to-noise ratio caused by the significant increase of the thermal noise. In fact, when the temperature further rises, TLS tends to fully saturate which decreases its effects. However, the total noise keeps increasing due to thermal noise which becomes dominant. In this case, the noise spectrum follows the Lorentzian function of white noise. Thus, the energy-resolving power magnitude is mainly limited by TLS noise when it is present and otherwise, by the signal-to-noise ratio. In FIG. 3, we overlay $E/\Delta E$ measured at 405 nm of four MKIDs, with two different sizes mentioned above per thickness, on the residual frequency shift $\Delta f_r/f_r$ as a function of bath temperature. The latter is measured in dark and it indicates the equilibrium state of MKIDs for a given temperature before being hit by photons. As reported elsewhere, a smaller meander size[20] combined with a lower T_c improves the energy-resolving power. We can also see that the wider temperature range where $E/\Delta E$ is optimal for the $TiN_{3.8K}$ MKID is due to its larger T_c. For example, with the $TiN_{3.8K}$ MKID, we can see that $E/\Delta E \geq 2$ up to 550 mK and $\sim$ 1.5-1 up to 700 mK are achieved.

In conclusion, we have demonstrated the capability of stoichiometric TiN-based MKIDs to operate in single photon mode. The obtained energy-resolving power $E/\Delta E$ is comparable to that of sub-stoichiometric TiN[18] or multilayer TiN/Ti/TiN. Furthermore, it can operate at a higher bath temperature well beyond 300 mK, up to 700 mK. On the other hand, we found out that $E/\Delta E$ shows an optimum with the bath temperature, between two noise minima, that of evanescent TLS and that of increasing thermal noise. In addition to a better understanding of the energy-resolving power-noise relationship, these results allow to consider the use of sensitive stoichiometric TiN-based MKIDs featuring T_c > 2K that will pave the way for the use of modest cryogenic systems such as sorption coolers to operate above 300 mK.

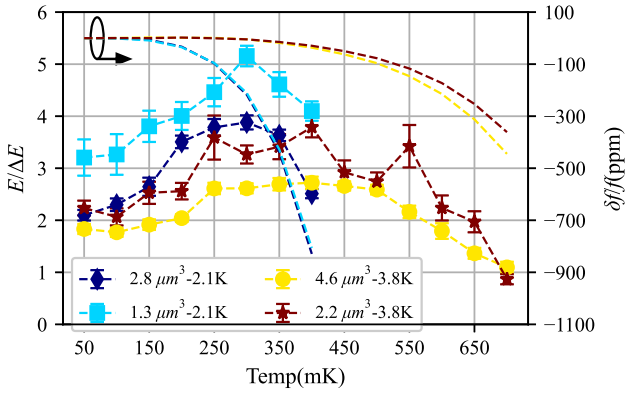

FIG. 3. Evolution of the energy-resolving power $R = E/\Delta E$ along with residual frequency shift $\Delta f_r/f_r$ as a function of bath temperature of four MKIDs illumintated at 405 nm. The corresponding frequencies are 2.625, 3.137 GHz made of $TiN_{2.1K}$ 15 nm-thick and 3.128, 4.078 GHz made of $TiN_{3.8K}$ 25 nm-thick.

ACKNOWLEDGMENTS

This work is supported by the European Research Council (ERC) and the french space agency (CNES).

[1] P. K. Day, H. G. LeDuc, B. A. Mazin, A. Vayonakis, and J. Zmuidzinas, Nature **425** (2003), 10.1038/nature02037.
[2] J. C. Eyken, M. J. Strader, A. B. Walter, S. R. Meeker, P. Szypryt, C. Stoughton, K. O'Brien, D. Marsden, N. K. Rice, Y. Lin, and B. A. Mazin, Astrophysical Journal, Supplement Series **219** (2015), 10.1088/0067-0049/219/1/14.
[3] A. B. Walter, N. Fruitwala, S. Steiger, J. I. Bailey, N. Zobrist, N. Swimmer, I. Lipartito, J. P. Smith, S. R. Meeker, C. Bockstiegel, G. Coiffard, R. Dodkins, P. Szypryt, K. K. Davis, M. Daal, B. Bumble, G. Collura, O. Guyon, J. Lozi, S. Vievard, N. Jovanovic, F. Martinache, T. Currie, and B. A. Mazin, Publications of the Astronomical Society of the Pacific **132** (2020), 10.1088/1538-3873/ab
[4] R. Adam, M. Arnaud, I. Bartalucci, P. Ade, P. André, A. Beelen, A. Benoît, A. Bideaud, N. Billot, H. Bourdin, O. Bourrion, M. Calvo, A. Catalano, G. Coiffard, B. Comis, A. D'Addabbo, F. X. Désert, S. Doyle, C. Ferrari, J. Goupy, C. Kramer, G. Lagache, S. Leclercq, J. F. Macías-Pérez, S. Maurogordato, P. Mauskopf, F. Mayet, A. Monfardini, F. Pajot, E. Pascale, L. Perotto, G. Pisano, E. Pointecouteau, N. Ponthieu, G. W. Pratt, V. Revéret, A. Ritacco, L. Rodriguez, C. Romero, F. Ruppin, K. Schuster, A. Sievers, S. Triqueneaux, C. Tucker, and R. Zylka, Astronomy and Astrophysics **606** (2017), 10.1051/0004-6361/201629810.
[5] M. J. Strader, A. M. Archibald, S. R. Meeker, P. Szypryt, A. B. Walter, J. C. van Eyken, G. Ulbricht, C. Stoughton, B. Bumble, D. L. Kaplan, and B. A. Mazin, Monthly Notices of the Royal Astronomical Society **459** (2016), 10.1093/mnras/stw663.
[6] A. Endo, R. M. Janssen, P. J. D. Visser, T. M. Klapwijk, P. V. D. Werf, J. J. Baselmans, S. J. Yates, L. Ferrari, A. M. Baryshev, and A. M. Baryshev (2012).
[7] M. Calvo, A. Benoît, A. Catalano, J. Goupy, A. Monfardini, N. Ponthieu, E. Barria, G. Bres, M. Grollier, G. Garde, J. P. Leggeri, G. Pont, S. Triqueneaux, R. Adam, O. Bourrion, J. F. Macías-Pérez, M. Rebolo, A. Ritacco,

J. P. Scordilis, D. Tourres, A. Adane, G. Coiffard, S. Leclercq, F. X. Désert, S. Doyle, P. Mauskopf, C. Tucker, P. Ade, P. André, A. Beelen, B. Belier, A. Bideaud, N. Billot, B. Comis, A. D'Addabbo, C. Kramer, J. Martino, F. Mayet, F. Pajot, E. Pascale, L. Perotto, V. Revéret, A. Ritacco, L. Rodriguez, G. Savini, K. Schuster, A. Sievers, and R. Zylka, Journal of Low Temperature Physics **184** (2016), 10.1007/s10909-016-1582-0.

[8] A. Ritacco, J. F. Macas-Pérez, N. Ponthieu, R. Adam, P. Ade, P. André, J. Aumont, A. Beelen, A. Benoit, A. Bideaud, N. Billot, O. Bourrion, A. Bracco, M. Calvo, A. Catalano, G. Coiffard, B. Comis, A. D'Addabbo, M. D. Petris, F. X. Désert, S. Doyle, J. Goupy, C. Kramer, G. Lagache, S. Leclercq, J. F. Lestrade, P. Mauskopf, F. Mayet, A. Maury, A. Monfardini, F. Pajot, E. Pascale, L. Perotto, G. Pisano, M. Rebolo-Iglesias, V. Revéret, L. Rodriguez, C. Romero, H. Roussel, F. Ruppin, K. Schuster, A. Sievers, G. Siringo, C. Thum, S. Triqueneaux, C. Tucker, H. Wiesemeyer, and R. Zylka, Astronomy and Astrophysics **616** (2018), 10.1051/0004-6361/201731551.

[9] P. Szypryt, S. R. Meeker, G. Coiffard, N. Fruitwala, B. Bumble, G. Ulbricht, A. B. Walter, M. Daal, C. Bockstiegel, G. Collura, N. Zobrist, I. Lipartito, and B. A. Mazin, Optics Express **25** (2017), 10.1364/oe.25.025894.

[10] G. Ulbricht, B. A. Mazin, P. Szypryt, A. B. Walter, C. Bockstiegel, and B. Bumble, Applied Physics Letters **106** (2015), 10.1063/1.4923096.

[11] A. Giachero, A. Cruciani, A. D'Addabbo, P. K. Day, S. D. Domizio, M. Faverzani, E. Ferri, B. Margesin, M. Martinez, R. Mezzena, L. Minutolo, A. Nucciotti, A. Puiu, and M. Vignati, Journal of Low Temperature Physics **193** (2018), 10.1007/s10909-018-2043-8.

[12] P. Szypryt, B. A. Mazin, G. Ulbricht, B. Bumble, S. R. Meeker, C. Bockstiegel, and A. B. Walter, Applied Physics Letters **109** (2016), 10.1063/1.4964665.

[13] N. Zobrist, B. H. Eom, P. Day, B. A. Mazin, S. R. Meeker, B. Bumble, H. G. Leduc, G. Coiffard, P. Szypryt, N. Fruitwala, I. Lipartito, and C. Bockstiegel, Applied Physics Letters **115** (2019), 10.1063/1.5098469.

[14] K. Kouwenhoven, D. Fan, E. Biancalani, S. A. de Rooij, T. Karim, C. S. Smith, V. Murugesan, D. J. Thoen, J. J. Baselmans, and P. J. de Visser, Phys. Rev. Appl. **19**, 034007 (2023).

[15] H. G. Leduc, B. Bumble, P. K. Day, B. H. Eom, J. Gao, S. Golwala, B. A. Mazin, S. McHugh, A. Merrill, D. C. Moore, O. Noroozian, A. D. Turner, and J. Zmuidzinas, Applied Physics Letters **97** (2010), 10.1063/1.3480420.

[16] M. R. Vissers, J. Gao, M. Sandberg, S. M. Duff, D. S. Wisbey, K. D. Irwin, and D. P. Pappas, Applied Physics Letters **102** (2013), 10.1063/1.4804286.

[17] F. Boussaha, S. Beldi, A. Monfardini, J. Hu, M. Calvo, C. Chaumont, F. Levy-Bertrand, T. Vacelet, A. Traini, J. Firminy, M. Piat, and F. Reix, Journal of Low Temperature Physics **199** (2020), 10.1007/s10909-019-02309-0.

[18] B. A. Mazin, B. Bumble, S. R. Meeker, K. O'Brien, S. McHugh, and E. Langman, Optics Express **20** (2012), 10.1364/oe.20.001503.

[19] J. Gao, M. R. Vissers, M. O. Sandberg, F. C. D. Silva, S. W. Nam, D. P. Pappas, D. S. Wisbey, E. C. Langman, S. R. Meeker, B. A. Mazin, H. G. Leduc, J. Zmuidzinas, and K. D. Irwin, Applied Physics Letters **101** (2012), 10.1063/1.4756916.

[20] W. Guo, X. Liu, Y. Wang, Q. Wei, L. F. Wei, J. Hubmayr, J. Fowler, J. Ullom, L. Vale, M. R. Vissers, and J. Gao, Applied Physics Letters **110** (2017), 10.1063/1.4984134.

[21] M. Faverzani, E. Ferri, A. Giachero, C. Giordano, B. Margesin, R. Mezzena, A. Nucciotti, and A. Puiu, Superconductor Science and Technology **33** (2020), 10.1088/1361-6668/ab7435.

[22] J. Hu, F. Boussaha, J. M. Martin, P. Nicaise, C. Chaumont, S. Beldi, M. Piat, and P. Bonifacio, Applied Physics Letters **119** (2021), 10.1063/5.0074103.

[23] J. Hu, M. Salatino, A. Traini, C. Chaumont, F. Boussaha, C. Goupil, and M. Piat, Journal of Low Temperature Physics **199** (2020), 10.1007/s10909-019-02313-4.

[24] N. Zobrist, W. H. Clay, G. Coiffard, M. Daal, N. Swimmer, P. Day, and B. A. Mazin, Physical Review Letters **129**, 017701 (2022).

[25] P. J. De Visser, S. A. De Rooij, V. Murugesan, D. J. Thoen, and J. J. Baselmans, Physical Review Applied **16**, 034051 (2021).

[26] S. Beldi, F. Boussaha, J. Hu, A. Monfardini, A. Traini, F. Levy-Bertrand, C. Chaumont, M. Gonzales, J. Firminy, F. Reix, M. Rosticher, S. Mignot, M. Piat, and P. Bonifacio, Optics Express **27** (2019), 10.1364/oe.27.013319.

[27] J. Hubmayr, J. Beall, D. Becker, H. M. Cho, M. Devlin, B. Dober, C. Groppi, G. C. Hilton, K. D. Irwin, D. Li, P. Mauskopf, D. P. Pappas, J. Van Lanen, M. R. Vissers, Y. Wang, L. F. Wei, and J. Gao, Applied Physics Letters **106**, 073505 (2015).